
Greedy inference with layers of lazy maps

Daniele Bigoni

Massachusetts Institute of Technology
Cambridge, MA 02139 USA
dabi@mit.edu

Olivier Zahm

Université Grenoble Alpes, CNRS, INRIA, LJK
38000 Grenoble, France
olivier.zahm@inria.fr

Alessio Spantini

Massachusetts Institute of Technology
Cambridge, MA 02139 USA
alessio.spantini@gmail.com

Youssef Marzouk

Massachusetts Institute of Technology
Cambridge, MA 02139 USA
ymarz@mit.edu

Abstract

We propose a framework for the greedy approximation of high-dimensional Bayesian inference problems, through the composition of multiple *low-dimensional* transport maps or flows. Our framework operates recursively on a sequence of “residual” distributions, given by pulling back the posterior through the previously computed transport maps. The action of each map is confined to a low-dimensional subspace that we identify by minimizing an error bound. At each step, our approach thus identifies (i) a relevant subspace of the residual distribution, and (ii) a low-dimensional transformation between a restriction of the residual onto this subspace and a standard Gaussian. We prove weak convergence of the approach to the posterior distribution, and we demonstrate the algorithm on a range of challenging inference problems in differential equations and spatial statistics.

1 Introduction

Inference in the Bayesian setting typically requires the computation of integrals $\int f d\pi$ over an *intractable* posterior distribution, whose density¹ π is known up to a normalizing constant. A useful approach to this problem involves constructing a deterministic nonlinear transformation, i.e., a *transport map* [40], that induces a coupling of π with a tractable distribution ρ (e.g., a standard Gaussian). More formally, we seek a map T that pushes forward ρ to π , written as $T_{\#}\rho = \pi$, such that the change of variables $\int f d\pi = \int f \circ T d\rho$ makes integration tractable.

Many constructions for such maps have been developed in recent years. Triangular maps [3, 21, 32] are sufficiently general to couple any absolutely continuous pair of distributions (ρ, π) , and their numerical approximations have been investigated in [19, 26, 28, 36]. Other constructions write T as a composition of simpler parameterized functions: these include normalizing flows [13, 30, 37], autoregressive flows [20], and neural ordinary differential equations [8, 14]. Stein variational methods [12, 23, 24] provide a nonparametric way of constructing T as a composition of functions lying in a chosen RKHS. Some of these methods have actually been proposed for density estimation (Gaussianizing a distribution from which one has drawn samples, via the action of a map $S = T^{-1}$ [22, 38]), while others have been developed for variational inference (approximating π by $T_{\#}\rho$, typically in the sense of Kullback–Leibler (KL) divergence), but these two problems are tightly linked as long as T is invertible.

¹In this paper, we only consider distributions that are absolutely continuous with respect to the Lebesgue measure on \mathbb{R}^d , and thus will use the notation π to denote both the distribution and its associated density.

Many of the methods mentioned above (with exceptions, e.g., Stein methods) are all-at-once: given some parameterized ansatz for the map, they solve a large and potentially challenging optimization problem for all the parameters simultaneously. More generally, it is difficult to represent expressive maps in high dimensions: parameterized triangular maps on \mathbb{R}^d , for example, must describe d -variate functions and thus immediately encounter the curse of dimensionality. Other flows involve particular ansatzes that limit their generality. Similarly, kernel-based methods lose expressiveness in high dimensions [7, 12]. Yet one of the key advantages of transport is the potential for iterative approximation using the *pullback distribution*: any invertible/bijective map preserves information about the target distribution π , and hence recursive—even greedy—approaches, applied to the pullback of π through imperfect maps, could be effective. In this paper we exploit the interplay between such approximations and low-dimensional structure.

We propose a new greedy framework for variational inference, based on compositions of low-dimensional maps. The maps are low-dimensional in that each acts non-trivially only on a low-dimensional subspace of the parameter space; thus they are termed “lazy.” We identify the maps and subspaces sequentially, by greedily minimizing a bound on the KL divergence between π and its approximation, given constraints on the computational effort at each step. The bound itself follows from logarithmic Sobolev inequalities (see [42]) relating the KL divergence to gradients of the target density. We prove weak convergence of this approach to the target distribution, given even suboptimal choices of the subspace. Within this framework, there is considerable flexibility. The complexity of the map, and hence the computational effort, can be tailored at each iteration. Moreover, each lazy map can be approximated by any invertible transformation; while here we do so using lazy triangular maps, one could instead use lazy maps obtained via Stein variational methods or normalizing flows.

We also emphasize that our overall approach does not require any *global* low dimensionality in the likelihood function (as in [7, 11], for example); rather, it can converge even for maps that act on a single direction at a time, despite π and ρ differing in all directions.

Preliminaries. We will consider target distributions with densities π on \mathbb{R}^d that are differentiable almost everywhere and that can be evaluated up to a normalizing constant. Such a target will often be the posterior of a Bayesian inference problem, e.g.,

$$\pi(x) := p(x|y) \propto \mathcal{L}_y(x)\pi_0(x), \quad (1)$$

where $\mathcal{L}_y(x) := p(y|x)$ is the likelihood function and π_0 is the prior. ρ will denote the standard Gaussian density on \mathbb{R}^d . We will consider maps $T : \mathbb{R}^d \rightarrow \mathbb{R}^d$ that are diffeomorphisms,² and with some abuse of notation, we will write the pushforward density of ρ under T as $T_{\#}\rho(x) := \rho \circ T^{-1}(x)|\nabla T^{-1}(x)|$. We will frequently also use the notion of a *pullback* distribution or density, written as $T^{\#}\pi := (T^{-1})_{\#}\pi$.

Our goal is to find a map T that satisfies $\mathcal{D}_{\text{KL}}(\pi||T_{\#}\rho) \leq \varepsilon$ for some prescribed tolerance $\varepsilon > 0$. In Section 2 we show how to build a single map in the “lazy” format described above. However, the map complexity needed to satisfy the prescribed tolerance might be large if ε is too small. We thus show in Section 3 how to improve our approximations by greedily composing many lazy maps.

2 Lazy maps

Given a unitary matrix $U \in \mathbb{R}^{d \times d}$ and an integer $r \leq d$, let $\mathcal{T}_r(U)$ be the set that contains all the maps $T : \mathbb{R}^d \rightarrow \mathbb{R}^d$ of the form

$$T(z) = U_r \tau(z_1, \dots, z_r) + U_{\perp} z_{\perp} \quad (2)$$

for some diffeomorphism $\tau : \mathbb{R}^r \rightarrow \mathbb{R}^r$. Here $U_r \in \mathbb{R}^{d \times r}$ and $U_{\perp} \in \mathbb{R}^{d \times (d-r)}$ are the matrices containing respectively the r first and the $d-r$ last columns of U , and $z_{\perp} = (z_{r+1}, \dots, z_d)$. Any map $T \in \mathcal{T}_r(U)$ is called a *lazy map* with rank bounded by r , as it is nonlinear only with respect to the first r inputs variables z_1, \dots, z_r and the nonlinearity is contained in the low-dimensional subspace $\text{range}(U_r)$. The next proposition gives a characterization of all the densities $T_{\#}\rho$ when $T \in \mathcal{T}_r(U)$.

²In general T does not need to be a diffeomorphism, but only a particular invertible map; see Appendix B for more details. The distributions we will consider in this paper, however, fulfill the necessary conditions for T to be differentiable almost everywhere.

Proposition 1 (Characterization of lazy maps). *Let $U \in \mathbb{R}^{d \times d}$ be a unitary matrix and let $r \leq d$. Then for any lazy map $T \in \mathcal{T}_r(U)$, there exists a strictly positive function $f : \mathbb{R}^r \rightarrow \mathbb{R}_{>0}$ such that*

$$T_{\sharp}\rho(x) = f(U_r^\top x)\rho(x), \quad (3)$$

for all $x \in \mathbb{R}^d$ where ρ is the density of the standard normal distribution. Conversely, any probability density function of the form $f(U_r^\top x)\rho(x)$ for some $f : \mathbb{R}^r \rightarrow \mathbb{R}_{>0}$ admits a representation as in (3) for some $T \in \mathcal{T}_r(U)$.

The proof is given in Appendix A.1. In particular, applying Proposition 1 to (1): if the prior distribution is $\pi_0 = \rho$ and if the likelihood function is of the form of $\mathcal{L}_y(x) = f(U_r^\top x)$, then there exists a lazy map $T \in \mathcal{T}_r(U)$ that exactly recovers the posterior density $T_{\sharp}\rho = \pi$. Following [42, Section 2.1], we have

$$\mathcal{D}_{\text{KL}}(\pi||T_{\sharp}\rho) = \mathcal{D}_{\text{KL}}(\pi||T_{\sharp}^*\rho) + \mathcal{D}_{\text{KL}}(T_{\sharp}^*\rho||T_{\sharp}\rho), \quad (4)$$

where $T^* \in \mathcal{T}_r(U)$ is such that $T_{\sharp}^*\rho(x) = f^*(U_r^\top x)\rho(x)$ and f^* is defined by the conditional expectation $f^*(y_r) = \mathbb{E} \left[\frac{\pi(X)}{\rho(X)} | U_r^\top X = y_r \right]$ with $X \sim \rho$. Because $\mathcal{D}_{\text{KL}}(T_{\sharp}^*\rho||T_{\sharp}\rho) \geq 0$, Equation (4) shows that T^* is a minimizer of $\mathcal{D}_{\text{KL}}(\pi||T_{\sharp}\rho)$ over $T \in \mathcal{T}_r(U)$. Following [18], one can show

$$\mathcal{D}_{\text{KL}}(\pi||T_{\sharp}^*\rho) = \mathcal{D}_{\text{KL}}(\pi||\rho) - \mathcal{D}_{\text{KL}}((U_r^\top)_{\sharp}\pi||\rho_r), \quad (5)$$

where ρ_r is the density of the standard normal distribution on \mathbb{R}^r and $(U_r^\top)_{\sharp}\pi$ is the marginal density of π with respect to U_r , meaning the density of $U_r^\top X$ with $X \sim \pi$. Equation (5) shows that, for fixed r , minimizing $\mathcal{D}_{\text{KL}}(\pi||T_{\sharp}^*\rho)$ over U is the same as finding the most non-Gaussian marginal $(U_r^\top)_{\sharp}\pi$. Such an optimal U can be difficult to find in practice. The next proposition gives a useful bound on $\mathcal{D}_{\text{KL}}(\pi||T_{\sharp}^*\rho)$, which we will use to construct a suboptimal U . Proof is given in Appendix A.2.

Proposition 2. *Let $(\lambda_i, u_i) \in \mathbb{R}_{>0} \times \mathbb{R}^d$ be the i -th eigenpair of the eigenvalue problem $Hu_i = \lambda_i u_i$ where $H = \int (\nabla \log \frac{\pi}{\rho})(\nabla \log \frac{\pi}{\rho})^\top d\pi$. Let $U = [u_1, \dots, u_d] \in \mathbb{R}^{d \times d}$ be the matrix containing the eigenvectors of H . Then for any $r \leq d$ we have*

$$\mathcal{D}_{\text{KL}}(\pi||T_{\sharp}^*\rho) \leq \frac{1}{2}(\lambda_{r+1} + \dots + \lambda_d). \quad (6)$$

Proposition 2 suggests constructing U as the matrix containing the eigenvectors of $H = \int (\nabla \log \frac{\pi}{\rho})(\nabla \log \frac{\pi}{\rho})^\top d\pi$ and choosing r to be the smallest integer such that the left-hand side of (6) is below ε . A fast decay in the spectrum of H ensures reaching the desired tolerance ε with $r \ll d$. In practice, however, this might not be the case either because ε is too small or because the spectrum of H does not decay quickly enough. Since the complexity for constructing the lazy map strongly depends on r , we bound r by some $r_{\max} \ll d$ that corresponds to the maximal computational budget one can afford in constructing T . This procedure is summarized in Algorithm 1.

Algorithm 1 Construction of a lazy map.

- 1: **procedure** LAZYMAP($\pi, \rho, \varepsilon, r_{\max}$)
 - 2: Compute $H = \int (\nabla \log \frac{\pi}{\rho})(\nabla \log \frac{\pi}{\rho})^\top d\pi$
 - 3: Solve the eigenvalue problem $Hu_i = \lambda_i u_i$
 - 4: Let $r = r_{\max} \wedge \min\{r \leq d : \frac{1}{2} \sum_{i>r} \lambda_i \leq \varepsilon\}$ and assemble $U = [u_1, \dots, u_d]$.
 - 5: Find T solution to $\min_{T \in \mathcal{T}_r(U)} \mathcal{D}_{\text{KL}}(\pi||T_{\sharp}\rho)$
 - 6: **return** lazy map T
 - 7: **end procedure**
-

The practical implementation of Algorithm 1 relies on the discretization of steps 2 (i.e., the computation of H) and 5 (i.e., minimizing the KL divergence). In step 2, direct Monte Carlo estimation of H requires generating samples from π , which is not feasible in practice. Following [42], one could use the importance sampling estimate $\tilde{H} = \frac{1}{K} \sum_{k=1}^K \omega_k (\nabla \log \frac{\pi}{\rho}(X_k)) (\nabla \log \frac{\pi}{\rho}(X_k))^\top$, where X_1, \dots, X_K are i.i.d. samples from ρ and where $\omega_k = \frac{\pi(X_k)}{\rho(X_k)} / (\sum_{k'=1}^K \frac{\pi(X_{k'})}{\rho(X_{k'})})$ are self-normalized weights. Such an estimate might have a huge variance when ρ is a poor approximation to the target π .

Algorithm 2 Compute layers of lazy maps

```

1: procedure LAYERSOFLAZYMAPS( $\pi, \rho, \varepsilon, r, \ell_{\max}$ )
2:   Set  $\pi_0 = \pi$  and  $\ell = 0$ 
3:   while  $\ell \leq \ell_{\max}$  and  $\frac{1}{2} \text{Tr}(H_\ell) \geq \varepsilon$  do
4:      $\ell \leftarrow \ell + 1$ 
5:     Compute  $T_\ell = \text{LAZYMAP}(\pi_{\ell-1}, \rho, 0, r)$  ▷ Algorithm 1
6:     Update  $\mathfrak{T}_\ell = \mathfrak{T}_{\ell-1} \circ T_\ell$ 
7:     Compute  $\pi_\ell = (\mathfrak{T}_\ell)_\# \pi$ 
8:     Compute  $H_\ell = \int (\nabla \log \frac{\pi_\ell}{\rho})(\nabla \log \frac{\pi_\ell}{\rho})^\top d\pi$ 
9:   end while
10:  return  $\mathfrak{T}_\ell = T_1 \circ \dots \circ T_\ell$ 
11: end procedure

```

In this case it is preferable to impose $\omega_k = 1$, which yields a more biased estimate \tilde{H}_ρ but with lower variance. As shown in Section 4 (see also the error bounds in [42, Sec. 3.3.2]), such an estimate still provides relevant information regarding the construction of U , and improves via the iterations described in Section 3.

At step 5 of Algorithm 1, we need to find the map $\tau : \mathbb{R}^r \rightarrow \mathbb{R}^r$ such that $T(z) = U_r \tau(z_1, \dots, z_r) + U_\perp z_\perp$ minimizes $\mathcal{D}_{\text{KL}}(\pi || T_\# \rho)$. Following the ideas in [1, 2, 19, 36], we seek τ in a parametric family of *monotone triangular* maps; details on this construction are given in Appendix B. As noted in [36], minimizing $\mathcal{D}_{\text{KL}}(\pi || T_\# \rho)$ over this class of parametric maps can be challenging because it is difficult to build good estimators for $\mathcal{D}_{\text{KL}}(\pi || T_\# \rho)$ when we cannot sample directly from π . In our setting we can only evaluate π up to a normalizing constant, and thus it is expedient to minimize the reverse KL divergence $\mathcal{D}_{\text{KL}}(T_\# \rho || \pi)$, as is typical in variational Bayesian methods—which here can be approximated using Monte Carlo sampling or quadrature from the tractable ρ . Details on the numerical implementation of Algorithm 1 are given in Appendix C. Though reversing the KL divergence in this step changes the approximation, we will show numerically that this computational strategy yields good results, ultimately controlling the KL divergence in both directions.

3 Layers of lazy maps

The restriction $r \leq r_{\max}$ in Algorithm 1 allows control over the computational cost of constructing the lazy map, but $\mathcal{D}_{\text{KL}}(\pi || T_\# \rho) \leq \varepsilon$ might not be satisfied. To compensate for this lack of accuracy while preserving low complexity, we propose to build a map \mathfrak{T}_ℓ as a composition of ℓ lazy maps

$$\mathfrak{T}_\ell = T_1 \circ \dots \circ T_\ell, \quad T_k \in \mathcal{T}_r(U^k),$$

where each T_k is a lazy map associated with a different unitary matrix $U^k \in \mathbb{R}^{d \times d}$. For simplicity we fix the same rank $r = r_{\max}$ for each T_k .

In general, the composition of lazy maps is not itself a lazy map. For example, there exists $U^1 \neq U^2$ such that $\mathfrak{T}_2 = T_1 \circ T_2$ might depend nonlinearly on each input variable and so it cannot be written as in (2). Notice also that there is no chance in general to write $(\mathfrak{T}_\ell)_\# \rho(x)$ as a product $f_1(U_r^{1\top} x) \dots f_\ell(U_r^{\ell\top} x) \rho(x)$; otherwise, by Proposition 1, \mathfrak{T}_ℓ would be a lazy map with rank bounded by $r\ell$. As a consequence, approximations of the form of $(\mathfrak{T}_\ell)_\# \rho$ are different than those constructed by projection pursuit [18].

We build the lazy maps in a greedy way. After $\ell - 1$ iterations, the composition of maps $\mathfrak{T}_{\ell-1} = T_1 \circ \dots \circ T_{\ell-1}$ have been constructed. We seek a unitary matrix $U^\ell \in \mathbb{R}^{d \times d}$ and a lazy map $T_\ell \in \mathcal{T}_r(U^\ell)$ such that $(\mathfrak{T}_{\ell-1} \circ T_\ell)_\# \rho$ is a better approximation to π than $(\mathfrak{T}_{\ell-1})_\# \rho$. Let

$$\pi_{\ell-1} = (\mathfrak{T}_{\ell-1})_\# \pi,$$

be the pullback density of π through $\mathfrak{T}_{\ell-1}$. Notice that $\mathcal{D}_{\text{KL}}(\pi || (\mathfrak{T}_{\ell-1} \circ T_\ell)_\# \rho) = \mathcal{D}_{\text{KL}}(\pi_{\ell-1} || (T_\ell)_\# \rho)$ so we can build T_ℓ using Algorithm 1 by replacing π by $\pi_{\ell-1}$ and ε by 0. Once this is done, we update the map $\mathfrak{T}_\ell = \mathfrak{T}_{\ell-1} \circ T_\ell$ and the residual density $\pi_\ell = (\mathfrak{T}_\ell)_\# \pi$ and we move to the next iteration $\ell \leftarrow \ell + 1$. We stop the iteration process when the error $\mathcal{D}_{\text{KL}}(\pi || (\mathfrak{T}_\ell)_\# \rho)$ falls below ε . Proposition 2 applied with π_ℓ and $r = 0$ allows writing $\mathcal{D}_{\text{KL}}(\pi || (\mathfrak{T}_\ell)_\# \rho) = \mathcal{D}_{\text{KL}}(\pi_\ell || \rho) \leq \frac{1}{2}(\lambda_1 + \dots + \lambda_d) =$

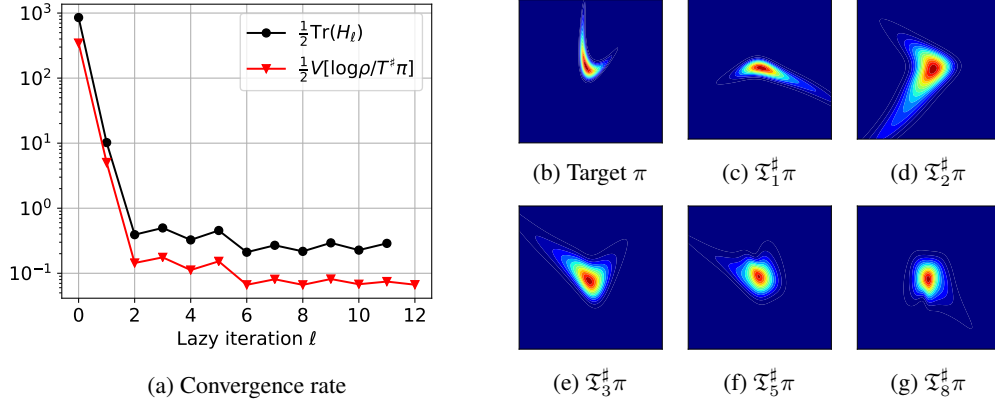


Figure 1: Convergence of the algorithm for the approximation of the rotated banana distribution. (a): decay rate of the bound $\frac{1}{2}\text{Tr}(H_\ell)$ of the KL-divergence $\mathcal{D}_{\text{KL}}(\pi \|\mathfrak{T}_{\ell^\sharp} \rho)$ and of its asymptotic approximation $\frac{1}{2}\mathbb{V}_\rho[\log \rho / \mathfrak{T}_{\ell^\sharp} \pi]$. (b): the target density π . (c-g): the target distribution is progressively Gaussianized by the maps \mathfrak{T}_ℓ .

$\frac{1}{2}\text{Tr}(H_\ell)$, where

$$H_\ell = \int \left(\nabla \log \frac{\pi_\ell}{\rho} \right) \left(\nabla \log \frac{\pi_\ell}{\rho} \right)^\top d\pi.$$

Hence, we can use $\frac{1}{2}\text{Tr}(H_\ell) \leq \varepsilon$ to stop the iteration. This greedy algorithm is summarized in Algorithm 2. Details on the numerical implementation of this algorithm are given in Appendix C.

The next proposition gives a sufficient condition on U^ℓ to guarantee the convergence of this greedy algorithm. The proof is given in Appendix A.3.

Proposition 3. *Let U^1, U^2, \dots be a sequence of unitary matrices. For any $\ell \geq 1$, we let $T_\ell \in \mathcal{T}_r(U^\ell)$ be a lazy map that minimizes $\mathcal{D}_{\text{KL}}(\pi_{\ell-1} \|(T_\ell)_\sharp \rho)$, where $\pi_{\ell-1} = (T_1 \circ \dots \circ T_{\ell-1})^\sharp \pi$. If there exists $0 < t \leq 1$ such that for any $\ell \geq 1$*

$$\mathcal{D}_{\text{KL}}((U_r^{\ell\top})_\sharp \pi_{\ell-1} \|\rho_r) \geq t \sup_{\substack{U \in \mathbb{R}^{d \times d} \\ \text{s.t. } UU^\top = I_d}} \mathcal{D}_{\text{KL}}((U_r^\top)_\sharp \pi_{\ell-1} \|\rho_r), \quad (7)$$

then $(T_1 \circ \dots \circ T_\ell)_\sharp \rho$ converges weakly to π .

Let us comment on the condition (7). Recall that the unitary matrix U that maximizes $\mathcal{D}_{\text{KL}}((U_r^\top)_\sharp \pi_{\ell-1} \|\rho_r)$ is optimal; see (5). By (7), the case $t = 1$ means that U^ℓ is optimal at each iteration. This corresponds to an *ideal* greedy algorithm. The case $0 < t < 1$ allows suboptimal choices for U^ℓ without losing the convergence property of the algorithm. Such a *weak* greedy algorithm converges even with a potentially crude selection of U^ℓ that corresponds to a t close to zero. This is why a crude approximation to H_ℓ is expected to be sufficient; see Section 4. Following [39], one can further relax the condition (7) by replacing t with a non-constant parameter t_ℓ which can go to zero “not too quickly” with respect to ℓ . This development is left for future work. Finally let us note that Proposition 3 does not require any constraints on r , so we have convergence even with $r = 1$. Of course, larger r yields faster convergence; see Section 4.

4 Numerical examples

We apply Algorithm 2 on a set of increasingly challenging inference problems. We monitor the convergence of the algorithm in two ways: (1) via the upper bound $\frac{1}{2}\text{Tr}(H_\ell)$ on the error $\mathcal{D}_{\text{KL}}(\pi \|\mathfrak{T}_{\ell^\sharp} \rho)$, where H_ℓ is replaced with its estimate \tilde{H}_ρ at step ℓ ; and (2) via the *variance diagnostic* $\frac{1}{2}\mathbb{V}_\rho[\log \rho / \mathfrak{T}_{\ell^\sharp} \pi]$ which is an asymptotic approximation of $\mathcal{D}_{\text{KL}}(\mathfrak{T}_{\ell^\sharp} \rho \|\pi)$ as $\mathfrak{T}_{\ell^\sharp} \rho \rightarrow \pi$ (see [28]). This latter quantity is easily computed, needing only samples from ρ , but is an approximation of the KL divergence in the *reverse* direction. Nevertheless, for the problems tackled here, we will

show empirically that this quantity is also bounded by $\frac{1}{2} \text{Tr}(H_\ell)$ in the spirit of Proposition 2. As a qualitative measure of performance, we plot 2D conditionals (“slices”) of $\mathfrak{T}_\ell^\# \pi$ which, at convergence, should be close to $\mathcal{N}(0, I_d)$. Finally, we will quantify the remaining bias in $\mathfrak{T}_\ell^\# \rho$ by reporting the acceptance rate and the effective sample size [41] of correlated samples from $\mathfrak{T}_\ell^\# \pi$ generated with MCMC algorithms—Metropolis-Hastings with a $\mathcal{N}(0, I_d)$ independence proposal [4, 31] (MH-ind) or with a preconditioned Crank-Nicolson proposal [10] (MH-pCN). A chain $\{\mathbf{Z}_i\}_i$ generated with this procedure can be used to obtain a chain with stationary distribution π , by applying the transformation $\{\mathbf{X}_i = \mathfrak{T}_\ell(\mathbf{Z}_i)\}_i$. This can be understood as a way of (asymptotically) de-biasing the variational approximation, or conversely as a way of preconditioning MCMC [29].

The algorithm is implemented³ in the TransportMaps framework [1]. The examples in Sections 4.1 and 4.2 have analytical likelihoods, while those in Sections 4.3 and 4.4 have likelihoods that depend on the solutions of partial differential equations (PDEs). The PDEs are discretized and solved using the packages FEniCS [25] and dolfin-adjoint [15]. The results in Sections 4.1, 4.2 and 4.4 are produced using one Intel[®] Core[™] i7-5930K CPU @ 3.50GHz. The results in Section 4.3 are obtained using 10 cores of the same type.

4.1 Lazy map construction step-by-step

We first apply the algorithm on the standard problem of approximating the rotated banana distribution $Q_\# \pi_{X_1, X_2}$ defined by $X_1 \sim \mathcal{N}(0.5, 0.8)$ and $X_2 | X_1 \sim \mathcal{N}(X_1^2, 0.2)$, and where Q is the linear map associated with a random rotation. Despite this being a two-dimensional problem that could be characterized by a degree-two lower triangular (full) map in a single step, we will restrict ourselves to the use of a composition of rank-1 lazy maps of degree 3 (i.e., diagonal maps with nonlinear first component). We use Gauss quadrature rules of order 10 for the discretization of the KL divergence and the approximation of H_ℓ ($m = 121$ in Algorithm 3 and 5).

Figure 1b shows the target distribution $\pi := \pi_{X_1, X_2}$. Figure 1a shows the convergence rate of the algorithm both in terms of residual power $\frac{1}{2} \text{Tr}(H)$ and in terms of variance diagnostic. After two iterations the algorithm has explored all the direction of \mathbb{R}^2 , leading to a fast improvement. The convergence stagnates once the trade-off between the complexity of \mathcal{T}_a and the accuracy of the quadrature has been saturated. Figures 1c–g show the progressive Gaussianization of the “residual” distributions $\mathfrak{T}_\ell^\# \pi$ for different iterations ℓ . To further confirm the quality of the approximation we generate an MCMC chain of length 10^4 , using MH-ind. The reported acceptance rate is 80.2% with the worst effective sample size being 21.3% of the total chain.

4.2 Log-Gaussian Cox process with sparse observations

We consider an inference problem in spatial statistics for a log-Gaussian Cox point process on a square domain $\mathcal{D} = [0, 1]^2$. This type of stochastic process is frequently used to model spatially aggregated point patterns [9, 16, 27, 33]. Following a configuration similar to [9, 27], we discretize \mathcal{D} into a 64×64 uniform grid, and denote by $\mathbf{s}_i \in \mathcal{D}$ the center of the i th cell, for $i = 1, \dots, d$, with $d = 64^2$. We consider a discrete stochastic process $(\mathbf{Y}_i)_{i=1}^d$, where \mathbf{Y}_i denotes the number of occurrences/points in the i th cell. Each \mathbf{Y}_i is modeled as a Poisson random variable with mean $\exp(\mathbf{Z}_i)/d$, where (\mathbf{Z}_i) is a Gaussian process with covariance $\text{Cov}(\mathbf{Z}_i, \mathbf{Z}_j) = \sigma^2 \exp(-\|\mathbf{s}_i - \mathbf{s}_j\|_2 / (64\beta))$ and mean $\mathbb{E}[\mathbf{Z}_i] = \mu$, for all $i = 1, \dots, d$. We consider the following values for the parameters: $\beta = 1/33$, $\sigma^2 = 1.91$, and $\mu = \log(126) - \sigma^2/2$. The (\mathbf{Y}_i) are assumed conditionally independent given the (latent) Gaussian field. For interpretability reasons, we also define the *intensity* process $(\mathbf{\Lambda}_i)_{i=1}^d$ as $\mathbf{\Lambda}_i = \exp(\mathbf{Z}_i)$, for $i = 1, \dots, d$.

The goal of this problem is to infer the posterior distribution of the latent process $\mathbf{\Lambda} := (\mathbf{\Lambda}_1, \dots, \mathbf{\Lambda}_n)$ given few sparse realizations of $\mathbf{Y} := (\mathbf{Y}_i)$ at $n = 30$ spatial locations $\mathbf{s}_{k_1}, \dots, \mathbf{s}_{k_n}$ shown in Figure 2a. We denote by $\mathbf{y}^* \in \mathbb{R}^n$ a realization of \mathbf{Y} obtained by sampling the latent Gaussian field according to its marginal distribution. Our target distribution is then: $\pi_{\mathbf{\Lambda} | \mathbf{Y}}(\boldsymbol{\lambda} | \mathbf{y}^*)$.

³The code can be retrieved at <http://bit.ly/2Q1e1XF>. Data for Sec. 4.2 is at <http://bit.ly/2HytQc0>. Data for Sec. 4.3 is at <http://bit.ly/2X09Ns8>. Data for Sec. 4.4 is at <http://bit.ly/2Eug5ZR>.

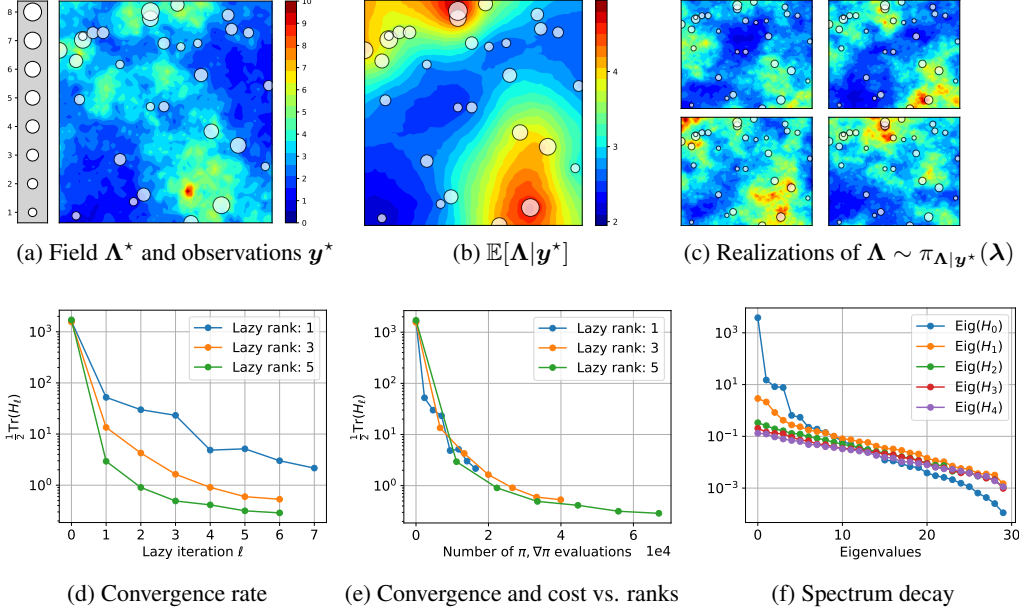


Figure 2: Application of the algorithm on the log-Gaussian Cox process distribution. Figure (a) shows the intensity field Λ^* used to generate the data \mathbf{y}^* (circles). Figures (b) shows the posterior expectation. Figure (c) shows few realizations from the posterior $\pi(\Lambda|\mathbf{y}^*)$. Figure (d) shows the convergence rate of the algorithm as a function of the iterations. Figure (e) shows the cost of the algorithm for different truncation ranks. Figure (f) shows the decay of the spectrum of H_ℓ for lazy maps with rank 5.

Since the posterior is nearly Gaussian, we will run three experiments with linear lazy maps and ranks $r = 1, 3, 5$. For the three experiments, the KL-divergence minimized for each lazy layer and the estimators of H_ℓ are discretized with $m = 100, 300, 500$ Monte Carlo samples respectively.

Figures 2b–c show the expectation and few realizations of the posterior, confirming the data provides some valuable information to recover the field Λ . Figures 2d–e show the convergence rate and the cost of the algorithm as new layers of lazy maps are added to \mathfrak{F}_ℓ . As we expect, the use of maps with higher ranks leads to faster convergence. On the other hand the computational cost per step increases—also due to the fact that we increase the sample size m as the rank increases. Figure 2f reveals the spirit of the algorithm: each lazy map trims away power from the top of the spectrum of H , which slowly flattens and decreases. To additionally confirm the quality of \mathfrak{F}_6 for lazy maps with rank 5, we generate an MCMC chain of length 10^4 using MH-ind. The reported acceptance rate is 72.6% with the worst effective sample size being 26.6% of the total chain.

4.3 Identification of the diffusion coefficient in an elliptic equation

We consider the problem of estimating the diffusion coefficient $e^{\kappa(\mathbf{x})}$ of an elliptic partial differential equation from sparse observations of the field $u(\mathbf{x})$ solving

$$\begin{cases} \nabla \cdot (e^{\kappa(\mathbf{x})} \nabla u(\mathbf{x})) = 0, & \text{for } \mathbf{x} \in \mathcal{D} := [0, 1]^2, \\ u(\mathbf{x}) = 0 \text{ for } \mathbf{x}_1 = 0, u(\mathbf{x}) = 1 \text{ for } \mathbf{x}_1 = 1, \frac{\partial u(\mathbf{x})}{\partial \mathbf{n}} = 0 \text{ for } \mathbf{x}_2 \in \{0, 1\}. \end{cases} \quad (8)$$

This PDE is discretized using finite elements over a uniform mesh of 51×51 nodes, leading to $d = 2601$ degrees of freedom. We denote by κ the discretized versions of the log-diffusion coefficient over this mesh.

Let \mathcal{F} be the map from the parameter κ to $n = 81$ uniformly distributed values of u collected at the locations shown in Figure 3a. Observations follow the model $\mathbf{y} = \mathcal{F}(\kappa) + \epsilon$, where $\epsilon \sim \mathcal{N}(0, \Sigma_{\text{obs}})$ and $\Sigma_{\text{obs}} := 10^{-3} I_d$. The coefficient κ is endowed with a Gaussian prior $\mathcal{N}(0, \Sigma)$ where Σ is the covariance of an Ornstein–Uhlenbeck process. For the observations \mathbf{y}^* associated to the parameter κ^* shown in Figure 3a, our target distribution is $\pi(\mathbf{z}) \propto \mathcal{L}_{\mathbf{y}^*}(\mathbf{z}) \rho(\mathbf{z})$, where $\kappa = \Sigma^{1/2} \mathbf{z}$.

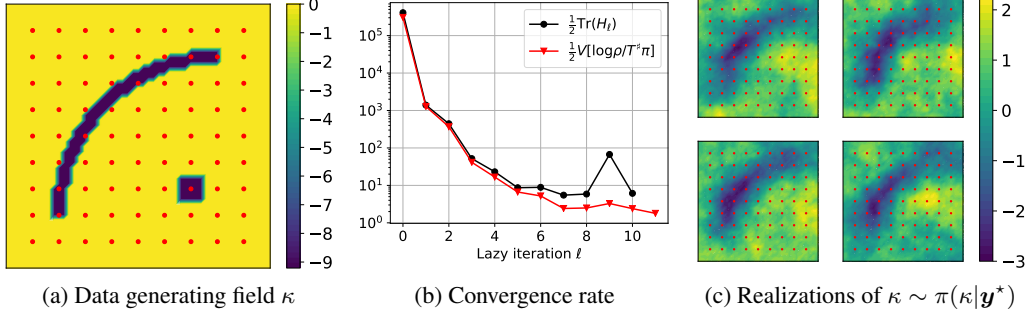


Figure 3: Application of the algorithm to the elliptic problem with unknown diffusion coefficient. Figure (a) shows the data generating field κ . Figure (b) shows the convergence of the algorithm as a function of the algorithm's iterations. Figure (c) shows four realizations drawn from the posterior distribution.

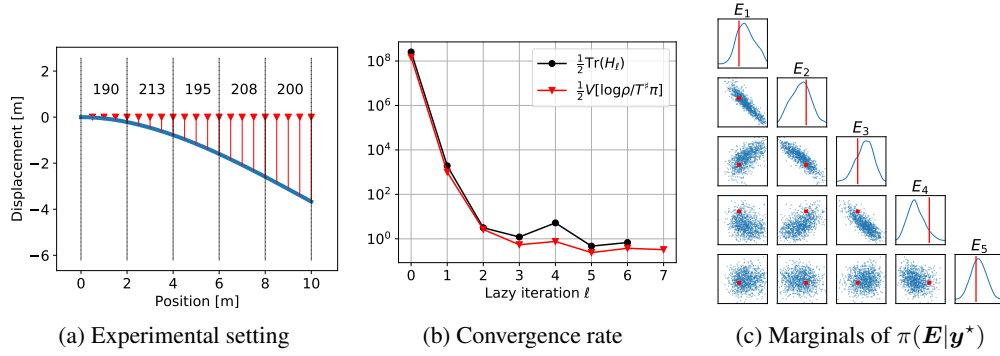


Figure 4: Application of the algorithm for the estimation of Young's modulus of a cantilever beam. Figure (a) shows the experimental setting, with the beam clamped at $x = 0$, the load applied at $x = l$, 20 sensors marked in red, and the true Young's modulus [GPa] for each segment. Figure (b) shows the convergence rate of the algorithm. Figure (c) shows marginals of the posterior distribution $\pi(\mathbf{E}|\mathbf{y}^*)$ along with the true values (red).

We discretize expectations appearing in the algorithm with $m = 500$ Monte Carlo samples. In order not to waste work in the early iterations we use linear maps of rank $r = 4$ for iterations $\ell = 1, \dots, 5$. Then we switch to maps of degree 2 and rank $r = 2$ for the remaining iterations. The algorithm is terminated when it stagnates due the lack of precision provided by the m samples; see Figure 3b. Randomly drawn realizations of κ in Figure 3c resemble the generating field. We confirm our results generating an MCMC chain of length 10^4 with MH-pCN and stepsize parameter $\beta = 0.5$. The reported acceptance rate is 28.22% with the worst, best and average effective sample sizes being 0.2%, 2.6% and 1.5% of the complete chain. For comparison, a direct application of MH-pCN with same β leads to an acceptance rate $< 0.4\%$. More details are provided in Appendix D.1.

4.4 Estimation of the Young's modulus of a cantilever beam

Here we consider the problem of estimating the Young's modulus $E(x)$ of an inhomogeneous cantilever beam, i.e., a beam clamped on one side ($x = 0$) and free on the other ($x = l$). The beam has a length of $l = 10$ m, a width of $w = 10$ cm and a thickness of $h = 30$ cm. Using Timoshenko's beam theory, the displacement $u(x)$ of the beam under the load $q(x)$ is modeled by the coupled PDEs

$$\begin{cases} \frac{d}{dx} \left[\frac{E(x)}{2(1+\nu)} \left(\varphi(x) - \frac{d}{dx} w(x) \right) \right] = \frac{q(x)}{\kappa A}, \\ \frac{d}{dx} \left(E(x) I \frac{d}{dx} \varphi(x) \right) = \kappa A \frac{E(x)}{2(1+\nu)} \left(\varphi(x) - \frac{d}{dx} w(x) \right), \end{cases} \quad (9)$$

where ν , κ , A , and I are parameters described in Appendix D.2. We consider a beam composed of $d = 5$ segments each of 2 m length made of different kinds of steel, with Young's moduli $\mathbf{E}^* = \{E_i\}_{i=1}^5 = \{190, 213, 195, 208, 200 \text{ GPa}\}$ respectively, and we run the virtual experiment

of applying a point mass of 5 kg at the tip of the beam. Observations \mathbf{y}^* of the displacement w are gathered at the locations shown in Figure 4a with a measurement noise of 1 mm. We endow \mathbf{E} with the prior $\pi(\mathbf{E}) = \mathcal{N}(200 \text{ GPa}, 25 \cdot I_5)$ and our goal is to characterize the posterior distribution $\pi(\mathbf{E}|\mathbf{y}^*) \propto \mathcal{L}_{\mathbf{y}^*}(\mathbf{E})\pi(\mathbf{E})$.

The algorithm is run with lazy maps of order 3 and rank 2. The expectations appearing in the algorithms are approximated using samples of size $m = 100$ from $\mathcal{N}(0, I_5)$. Figure 4 summarizes the results. We further confirm these results generating an MCMC chain of length 10^4 using MH-ind. The reported acceptance rate is 68.3% with the worst, best, and average effective sample sizes being 7.0%, 38.7%, and 20.1% of the complete chain. Further details regarding the problem setting and additional results are reported in Appendix D.2.

Acknowledgments

This work was supported in part by the US Department of Energy, Office of Advanced Scientific Computing Research, AEOLUS (Advances in Experimental Design, Optimal Control, and Learning for Uncertain Complex Systems) project. The authors also gratefully acknowledge support from the Inria associate team UNQUESTIONABLE.

References

- [1] D. Bigoni. TransportMaps. <http://transportmaps.mit.edu/>, 2016–2019.
- [2] D. Bigoni, A. Spantini, and Y. Marzouk. Adaptive construction of measure transports for Bayesian inference. *NIPS workshop on Approximate Inference*, 2016.
- [3] V. I. Bogachev, A. V. Kolesnikov, and K. V. Medvedev. Triangular transformations of measures. *Sbornik: Mathematics*, 196(3):309, 2005.
- [4] S. Brooks, A. Gelman, G. Jones, and X.-L. Meng. *Handbook of Markov Chain Monte Carlo*. CRC press, 2011.
- [5] C. G. Broyden. The Convergence of a Class of Double Rank Minimization Algorithms. Part {II}. *J. Inst. Math. Appl.*, 6:222, 1970.
- [6] G. Carlier, A. Galichon, and F. Santambrogio. From Knothe’s transport to Brenier’s map and a continuation method for optimal transport. *SIAM Journal on Mathematical Analysis*, 41(6):2554–2576, 2010.
- [7] P. Chen, K. Wu, J. Chen, T. O’Leary-Roseberry, and O. Ghattas. Projected Stein Variational Newton: A Fast and Scalable Bayesian Inference Method in High Dimensions. *arXiv e-prints*, Jan. 2019.
- [8] R. T. Q. Chen, Y. Rubanova, J. Bettencourt, and D. Duvenaud. Neural Ordinary Differential Equations. *NeurIPS*, 2018.
- [9] O. F. Christensen, G. O. Roberts, and J. S. Rosenthal. Scaling limits for the transient phase of local Metropolis-Hastings algorithms. *Journal of the Royal Statistical Society. Series B: Statistical Methodology*, 67(2):253–268, 2005.
- [10] S. L. Cotter, G. O. Roberts, A. M. Stuart, and D. White. MCMC Methods for Functions: Modifying Old Algorithms to Make Them Faster. *Statistical Science*, 28(3):424–446, 2013.
- [11] T. Cui, J. Martin, Y. Marzouk, A. Solonen, and A. Spantini. Likelihood-informed dimension reduction for nonlinear inverse problems. *Inverse Problems*, 30(11):114015, 2014.
- [12] G. Detommaso, T. Cui, A. Spantini, Y. Marzouk, and R. Scheichl. A Stein variational Newton method. *NeurIPS*, 2018.
- [13] L. Dinh, J. Sohl-Dickstein, and S. Bengio. Density estimation using real NVP. *arXiv:1605.08803*, 2016.
- [14] E. Dupont, A. Doucet, and Y. W. Teh. Augmented Neural ODEs. *arXiv preprint arXiv:1904.01681*, 2019.

- [15] P. E. Farrell, D. A. Ham, S. W. Funke, and M. E. Rognes. Automated Derivation of the Adjoint of High-Level Transient Finite Element Programs. *SIAM Journal on Scientific Computing*, 35(4):C369–C393, jan 2013.
- [16] M. Girolami and B. Calderhead. Riemann manifold Langevin and Hamiltonian Monte Carlo methods. *Journal of the Royal Statistical Society: Series B (Statistical Methodology)*, 73(2):123–214, 2011.
- [17] G. H. Golub and J. H. Welsch. Calculation of Gauss quadrature rules. *Mathematics of Computation*, 23(106):221–221, may 1969.
- [18] P. J. Huber. Projection pursuit. *The Annals of Statistics*, pages 435–475, 1985.
- [19] P. Jaini, K. A. Selby, and Y. Yu. Sum-of-Squares Polynomial Flow. *arXiv:1905.02325*, 2019.
- [20] D. P. Kingma, T. Salimans, R. Jozefowicz, X. Chen, I. Sutskever, and M. Welling. Improved variational inference with inverse autoregressive flow. In D. D. Lee, M. Sugiyama, U. V. Luxburg, I. Guyon, and R. Garnett, editors, *Advances in Neural Information Processing Systems 29*, pages 4743–4751. Curran Associates, Inc., 2016.
- [21] H. Knothe et al. Contributions to the theory of convex bodies. *The Michigan Mathematical Journal*, 4(1):39–52, 1957.
- [22] V. Laparra, G. Camps-Valls, and J. Malo. Iterative Gaussianization: from ICA to random rotations. *IEEE Transactions on Neural Networks*, 22(4):537–549, 2011.
- [23] Q. Liu. Stein variational gradient descent as gradient flow. In *Advances in neural information processing systems*, pages 3115–3123, 2017.
- [24] Q. Liu and D. Wang. Stein Variational Gradient Descent: A general purpose Bayesian inference algorithm. In *Advances in Neural Information Processing Systems*, pages 2370–2378, 2016.
- [25] A. Logg and G. N. Wells. Dolfin: Automated finite element computing. *ACM Transactions on Mathematical Software*, 37(2), 2010.
- [26] Y. Marzouk, T. Moselhy, M. Parno, and A. Spantini. Sampling via measure transport: An introduction. In *Handbook of Uncertainty Quantification*, R. Ghanem, D. Higdon, and H. Owhadi, editors. Springer, 2016.
- [27] J. Møller, A. R. Syversveen, and R. Waagepetersen. Log Gaussian Cox Processes. *Scandinavian Journal of Statistics*, 25(3):451–482, 1998.
- [28] T. Moselhy and Y. Marzouk. Bayesian inference with optimal maps. *Journal of Computational Physics*, 231(23):7815–7850, 2012.
- [29] M. Parno and Y. M. Marzouk. Transport map accelerated Markov chain Monte Carlo. *SIAM/ASA Journal on Uncertainty Quantification*, 6(2):645–682, 2018.
- [30] D. J. Rezende and S. Mohamed. Variational inference with normalizing flows. *arXiv:1505.05770*, 2015.
- [31] C. Robert and G. Casella. *Monte Carlo statistical methods*. Springer Science & Business Media, 2013.
- [32] M. Rosenblatt. Remarks on a multivariate transformation. *The Annals of Mathematical Statistics*, pages 470–472, 1952.
- [33] H. Rue, S. Martino, and N. Chopin. Approximate Bayesian inference for latent Gaussian models by using integrated nested Laplace approximations. *Journal of the Royal Statistical Society: Series B*, 71(2):319–392, 2009.
- [34] F. Santambrogio. *Optimal Transport for Applied Mathematicians*, volume 87. Springer, 2015.
- [35] S. Smolyak. Quadrature and interpolation formulas for tensor products of certain classes of functions. *Dokl. Akad. Nauk SSSR*, 1963.

- [36] A. Spantini, D. Bigoni, and Y. Marzouk. Inference via low-dimensional couplings. *The Journal of Machine Learning Research*, 19(1):2639–2709, 2018.
- [37] E. Tabak and C. V. Turner. A family of nonparametric density estimation algorithms. *Communications on Pure and Applied Mathematics*, 66(2):145–164, 2013.
- [38] E. G. Tabak, E. Vanden-Eijnden, et al. Density estimation by dual ascent of the log-likelihood. *Communications in Mathematical Sciences*, 8(1):217–233, 2010.
- [39] V. N. Temlyakov. Greedy approximation. *Acta Numerica*, 17:235–409, 2008.
- [40] C. Villani. *Optimal transport: old and new*, volume 338. Springer Science & Business Media, 2008.
- [41] U. Wolff. Monte Carlo errors with less errors. *Computer Physics Communications*, 156(2):143–153, 2004.
- [42] O. Zahm, T. Cui, K. Law, A. Spantini, and Y. Marzouk. Certified dimension reduction in nonlinear Bayesian inverse problems. *arXiv preprint arXiv:1807.03712*, 2018.

A Proofs

A.1 Proof of Proposition 1

We first show that for any $T \in \mathcal{T}_r(U)$ there exists a $f : \mathbb{R}^r \rightarrow \mathbb{R}_{>0}$ such that (3) holds. Let $T \in \mathcal{T}_r(U)$. Because T is a diffeomorphism we have $T_{\#}\rho(x) = \rho(T^{-1}(x))\det(\nabla T^{-1}(x))$. The inverse of T is given by

$$T^{-1}(x) = \begin{pmatrix} \tau^{-1}(U_r^T x) \\ U_{\perp}^T x \end{pmatrix},$$

so that $\det(\nabla T^{-1}(x)) = \det(\nabla \tau^{-1}(U_r^T x))$ and, because $\rho(x) \propto \exp(-\frac{1}{2}\|x\|_2^2)$, we have $\rho(T^{-1}(x)) \propto \rho(x) \exp(-\frac{1}{2}\|\tau^{-1}(U_r^T x)\|_2^2 + \frac{1}{2}\|U_r^T x\|_2^2)$. This yields (3) with $f(U_r^T x) = \exp(-\frac{1}{2}\|\tau^{-1}(U_r^T x)\|_2^2 + \frac{1}{2}\|U_r^T x\|_2^2)\det(\nabla \tau^{-1}(U_r^T x))$.

Now we show that for any function $f : \mathbb{R}^r \rightarrow \mathbb{R}_{>0}$ there exists a lazy map $T \in \mathcal{T}_r(U)$ such that (3) holds. Let $f : \mathbb{R}^r \rightarrow \mathbb{R}_{>0}$. Denote by ρ_r (resp. ρ_{\perp}) the density of the standard normal distribution on \mathbb{R}^r (resp. \mathbb{R}^{d-r}). Let $\tau : \mathbb{R}^r \rightarrow \mathbb{R}^r$ be a map that pushes forward ρ_r to π_r , where π_r is the probability density on \mathbb{R}^r defined by $\pi_r(y_r) \propto f(y_r)\rho_r(y_r)$. Such a map always exists because the support of π_r (and of ρ_r) is \mathbb{R}^r , see [40]. Consider the map $Q : \mathbb{R}^d \rightarrow \mathbb{R}^d$ defined by

$$Q(z) = \begin{pmatrix} \tau(z_1, \dots, z_r) \\ z_{\perp} \end{pmatrix}.$$

Because $\rho = \rho_r \otimes \rho_{\perp}$, we have $Q_{\#}\rho(y) = \tau_{\#}\rho_r(y_r)\rho(y_{\perp}) \propto f(y_r)\rho(y)$. Finally, the lazy map $T(z) = U_r \tau(z_1, \dots, z_r) + U_{\perp} z_{\perp} = UQ(z)$ satisfies $T_{\#}\rho(z) = U_{\#}(Q_{\#}\rho)(z) \propto f((U^T z)_r)\rho(U^T z) \propto f(U_r^T z)\rho(z)$. This concludes the proof.

A.2 Proof of Proposition 2

Corollary 1 in [42] allows us to write $\mathcal{D}_{\text{KL}}(\pi(x)||f^*(U_r^T x)\rho(x)) \leq \frac{\kappa}{2} \text{Tr}(\Gamma^{-1}(I_d - U_r U_r^T)H(I_d - U_r U_r^T))$ with $\kappa = 1$ and $\Gamma = I_d$, see [42, Example 1]. Because U is the matrix containing the first eigenvectors of H we have $\text{Tr}((I_d - U_r U_r^T)H(I_d - U_r U_r^T)) = \lambda_{r+1} + \dots + \lambda_d$.

A.3 Proof of Proposition 3

Let $R_{\ell} = \mathcal{D}_{\text{KL}}((U_r^{\ell T})_{\#}\pi_{\ell-1}||\rho_r)$. Replacing π by $\pi_{\ell-1}$ in (5) allows writing $\mathcal{D}_{\text{KL}}(\pi_{\ell-1}||(T_{\ell})_{\#}\rho) = \mathcal{D}_{\text{KL}}(\pi_{\ell-1}||\rho) - R_{\ell}$ so that

$$\mathcal{D}_{\text{KL}}(\pi_{\ell}||\rho) = \mathcal{D}_{\text{KL}}(\pi||\rho) - \sum_{k=1}^{\ell-1} R_k.$$

In particular R_k converges to 0 and, because of (7), we have

$$\sup_{\substack{U \in \mathbb{R}^{d \times d} \\ \text{s.t. } UU^T = I_d}} \mathcal{D}_{\text{KL}}((U_r^T)_\# \pi_{\ell-1} \| \rho_r) \xrightarrow{\ell \rightarrow \infty} 0.$$

By Proposition 14.2 in [18], $\pi_{\ell-1}$ converges weakly to ρ . Then $(T_1 \circ \dots \circ T_\ell)_\# \rho$ converges weakly to π .

B Triangular maps

There may exist many (indeed an infinity) of transport maps able to couple two arbitrary probability distributions. In optimal transport [40], a map is identified by minimizing some expected transportation cost, which represents the effort required to move mass from one location to another. In this work, we take an alternative approach and consider lower triangular transports,

$$T(\mathbf{x}) = \begin{bmatrix} T^{(1)}(x_1) \\ T^{(2)}(x_1, x_2) \\ \vdots \\ T^{(d)}(x_1, \dots, x_d) \end{bmatrix} \quad (10)$$

where each component $T^{(i)}$ is monotonically increasing with respect to x_i . We will identify these transports with the set $\mathcal{T}_> = \{T : \mathbb{R}^d \rightarrow \mathbb{R}^d \mid T \text{ is triangular and } \partial_{x_i} T_i > 0\}$. For any two distributions ρ and π on \mathbb{R}^d that admit densities with respect to Lebesgue measure (also denoted by ρ and π , respectively) there exists a unique transport $T \in \mathcal{T}_>$ such that $T_\# \rho = \pi$. This transport is known as the Knothe–Rosenblatt (KR) rearrangement [3, 6, 21, 32]. Because T is invertible, the density of the *pullback* measure $T^\# \pi$ is given by $T^\# \pi(\mathbf{x}) = \pi \circ T(\mathbf{x}) \det \nabla T(\mathbf{x})$, where $\det \nabla T(\mathbf{x})$ is defined by $\prod_{i=1}^d \partial_{x_i} T^{(i)}(\mathbf{x}_{1:i})$. We stress here that $\det \nabla T(\mathbf{x})$ is a definition, and T does not need to be differentiable. In fact, T inherits the same regularity as ρ and π , but no more [3, 34].

We consider semi-parametric approximations to maps in $\mathcal{T}_>$, i.e., we will consider the set $\mathcal{T}_>^\dagger \subset \mathcal{T}_>$ of maps $T : (\mathbf{a}, \mathbf{x}) \mapsto T[\mathbf{a}](\mathbf{x})$ defined by

$$T^{(i)}[\mathbf{c}_i, \mathbf{h}_i](\mathbf{x}) := c[\mathbf{c}_i](\mathbf{x}_{1:i-1}) + \int_0^{x_i} (h[\mathbf{h}_i](\mathbf{x}_{1:i-1}, t))^2 dt, \quad (11)$$

where $\mathbf{a} = \{(\mathbf{c}_i, \mathbf{h}_i)\}_{i=1}^d$, and (c, h) are in the span of a polynomial basis. The KR rearrangement between ρ and π can be obtained as the unique minimizer T^* of $\min_{T \in \mathcal{T}_>} \mathcal{D}_{\text{KL}}(T_\# \rho \| \pi) = \min_{T \in \mathcal{T}_>} \mathbb{E}_\rho[\log \rho / T^\# \pi]$. An approximation to it can be obtained by restricting the minimization over the set $\mathcal{T}_>^\dagger$ [2, 26, 28].

C Numerical algorithms

Algorithm 3 assembles the numerical approximation of $H_\nu = \int (\nabla \log \frac{\pi}{\rho})(\nabla \log \frac{\pi}{\rho})^\top d\nu$. In the following we will chose ν to be the reference distribution ρ , leading to H_ρ being a biased approximation of $H = \int (\nabla \log \frac{\pi}{\rho})(\nabla \log \frac{\pi}{\rho})^\top d\pi$. In the examples presented the number of samples m used for the approximation of \tilde{H}_ρ is chosen to be the same used for Algorithm 5, even though the type of quadrature may differ—e.g., Monte Carlo, Gauss quadrature[17], sparse grids [35], etc. This way the extra cost of computing \tilde{H}_ρ is equivalent to one gradient evaluation in the quasi-Newton method.

Algorithm 4 computes the eigenvectors U satisfying Proposition 2 and discerns between the subspace $\text{span}(U_r)$ of relevant directions and its orthogonal complement $\text{span}(U_\perp)$.

Algorithm 5 outlines the numerical solution of the variational problem

$$T[\mathbf{a}^*] = \arg \min_{T[\mathbf{a}] \in \mathcal{T}_\mathbf{a}} \mathcal{D}_{\text{KL}}(T[\mathbf{a}]_\# \rho \| \pi) \quad (12)$$

In the sake of simplicity we fix the complexity N of the semi-parametric map T described in Appendix B and the sample size m used in the discretization of the KL divergence. Alternatively one could

adaptively increase the complexity and the sample size to match a prescribed tolerance, following the procedure described in [2]. For all the examples presented in this work, the minimization problem is solved via the Broyden–Fletcher–Goldfarb–Shanno (BFGS) quasi-Newton method [5]. One could switch to a full Newton method if the Hessian of π or its action on a vector are available..

Algorithms 6 and 7 are the numerical counterparts of Algorithms 1 and 2 respectively.

Algorithm 3 Given the quadrature $(x_i, w_i)_{i=1}^m$ with respect to the distribution ν and the unnormalized density π , compute an approximation to $H_\nu = \int (\nabla \log \frac{\pi}{\rho})(\nabla \log \frac{\pi}{\rho})^\top d\nu$.

1: **procedure** COMPUTEH($(x_i, w_i)_{i=1}^m, \pi$)

2: Assemble

▷ Here $\rho = \mathcal{N}(0, \mathbf{I})$

$$\tilde{H}_\nu = \sum_{i=1}^m \left(\nabla_{\mathbf{x}} \log \frac{\pi}{\rho}(x_i) \right) \left(\nabla_{\mathbf{x}} \log \frac{\pi}{\rho}(x_i) \right)^T w_i$$

return \tilde{H}_ν

3: **end procedure**

Algorithm 4 Given the matrix $\tilde{H}_\rho \approx \int (\nabla \log \frac{\pi_\varepsilon}{\rho})(\nabla \log \frac{\pi_\varepsilon}{\rho})^\top d\rho$ and the tolerance ε , find the matrix $U := [U_r | U_\perp]$ that satisfies Proposition 2.

1: **procedure** COMPUTESUBSPACE($\tilde{H}_\rho, \varepsilon, r_{\max}$)

2: Solve the eigenvalue problem $\tilde{H}_\rho X = \Lambda X$

3: Let $r = r_{\max} \wedge \min\{r \leq d : \frac{1}{2} \sum_{i>r} \lambda_i \leq \varepsilon\}$

4: Define $U_r = [X_{:,1}, \dots, X_{:,r}]$ and $U_\perp = [X_{:,r+1}, \dots, X_{:,n}]$

5: **return** U_r, U_\perp, r

6: **end procedure**

Algorithm 5 Given the quadrature $(x_i, w_i)_{i=1}^m$ from the reference density $\mathcal{N}(0, I_d)$, the unnormalized target density π , a set of triangular monotone map $\mathcal{T}_{\mathbf{a}}$ parametrized by the set of coefficients $\mathbf{a} \in \mathbb{R}^N$ and a tolerance ε_{map} find the optimal coefficients \mathbf{a}^* such that $T[\mathbf{a}]_{\#}\rho \propto \pi$ by minimizing (12).

1: **procedure** COMPUTEMAP($(x_i, w_i)_{i=1}^m, \pi, \mathcal{T}_{\mathbf{a}}, \varepsilon_{\text{map}}$)

2: Solve (e.g., via a quasi-Newton or Newton method),

$$T[\mathbf{a}^*] = \arg \min_{T[\mathbf{a}] \in \mathcal{T}_{\mathbf{a}}} - \underbrace{\sum_{i=1}^m \left(\log \pi(T[\mathbf{a}](x_i)) + \sum_k \log \partial_k T[\mathbf{a}]^k(x_i) \right)}_{\mathcal{J}[\mathbf{a}]} w_i,$$

such that, e.g., $\|\nabla_{\mathbf{a}} \mathcal{J}[\mathbf{a}^*]\|_2 < \varepsilon_{\text{map}}$

3: **return** $T[\mathbf{a}^*]$

4: **end procedure**

Algorithm 6 Given the unnormalized density π , the matrix $\tilde{H}_\rho \approx \int (\nabla \log \frac{\pi_\ell}{\rho})(\nabla \log \frac{\pi_\ell}{\rho})^\top d\rho$, the rank truncation tolerance ε_r , the maximum rank r_{\max} , the number of samples m used to discretize expectations, the set of parametric triangular monotone maps $\mathcal{T}_\mathbf{a}$ and the target tolerance ε_{map} for the learning of the map τ , identify the optimal lazy map T .

- 1: **procedure** LAZYMAPCONSTRUCTION($\pi, \tilde{H}_\rho, \varepsilon_r, r_{\max}, m, \mathcal{T}_\mathbf{a}, \varepsilon_{\text{map}},$)
 - 2: $U_r, U_\perp, r \leftarrow \text{COMPUTESUBSPACE}(\tilde{H}_\rho, \varepsilon_r, r_{\max})$ ▷ Algorithm 4
 - 3: Define $\hat{\pi}(x) := (U_r|U_\perp)^\# \pi(x) = \pi \circ (U_r|U_\perp) x$
 - 4: Build the quadrature $(x_i, w_i)_{i=1}^m$ with respect to $\mathcal{N}(0, I_d)$
 - 5: Define $\mathcal{T}_{r,\mathbf{a}} = \left\{ T[\mathbf{a}](z) = [\tau[\mathbf{a}](z_1, \dots, z_r)^\top, z_{r+1}, \dots, z_d]^\top \mid \tau[\mathbf{a}] \in \mathcal{T}_\mathbf{a} \right\}$
 - 6: $T[\mathbf{a}^*] \leftarrow \text{COMPUTEMAP}((x_i, w_i)_{i=1}^m, \hat{\pi}, \mathcal{T}_{r,\mathbf{a}}, \varepsilon_{\text{map}})$ ▷ Algorithm 5
 - 7: Define $L(z) := (U_r|U_\perp) \circ T[\mathbf{a}](z)$
 - 8: **return** L
 - 9: **end procedure**
-

Algorithm 7 Given the target density π , a stopping tolerance ε and a maximum number of iterations ℓ_{\max} , computes layers of lazy maps with fixed rank r . See Algorithm 6 for the definition of the remaining arguments.

- 1: **procedure** LAYERSOFLAZYMAPSCONSTRUCTION($\pi, \varepsilon, r, \ell_{\max}, m, \mathcal{T}_\mathbf{a}, \varepsilon_{\text{map}})$
 - 2: Set $\pi_0 = \pi$ and $\ell = 0$
 - 3: Build the quadrature $(x_i, w_i)_{i=1}^m$ with respect to $\mathcal{N}(0, I_d)$
 - 4: Compute $\tilde{H}_{\rho,\ell} = \text{COMPUTE}H((x_i, w_i)_{i=1}^m, \pi_\ell)$
 - 5: **while** $\ell \leq \ell_{\max}$ and $\frac{1}{2} \text{Tr}(\tilde{H}_{\rho,\ell}) \geq \varepsilon$ **do**
 - 6: $\ell \leftarrow \ell + 1$
 - 7: $T_\ell \leftarrow \text{LAZYMAPCONSTRUCTION}(\pi_{\ell-1}, \tilde{H}_{\rho,\ell}, 0, r, m, \mathcal{T}_\mathbf{a}, \varepsilon_{\text{map}})$ ▷ Algorithm 6
 - 8: Update $\mathfrak{T}_\ell = \mathfrak{T}_{\ell-1} \circ T_\ell$
 - 9: Compute $\pi_\ell = (\mathfrak{T}_\ell)^\# \pi$
 - 10: Build the quadrature $(x_i, w_i)_{i=1}^m$ with respect to $\mathcal{N}(0, I_d)$
 - 11: Compute $\tilde{H}_{\rho,\ell} = \text{COMPUTE}H((x_i, w_i)_{i=1}^m, \pi_\ell)$
 - 12: **end while**
 - 13: **return** $\mathfrak{T}_\ell = T_1 \circ \dots \circ T_\ell$
 - 14: **end procedure**
-

D Additional material for the numerical examples

We collect here some additional details and results about the numerical examples.

D.1 Identification of the diffusion coefficient in an elliptic equation

Here we explain how the numerical discretization of the PDE enters the Bayesian inference formulation. We denote by \mathcal{S} the map $\kappa \mapsto u$, mapping the discretized coefficient to the numerical solution of equation 8. The observation map is defined by the operator $B_i(u) := \int_{\mathcal{D}} u \phi_i d\mathbf{x}$, where $\phi_i(\mathbf{x}) := \exp[-\|\mathbf{s}_i - \mathbf{x}\|_2^2 / (2\delta^2)] / \gamma_i$, $\{\mathbf{s}_i\}_{i=1}^n \in \mathcal{D}$ are observation locations, $\delta = 10^{-4}$, and γ_i are normalization constants so that $\int_{\mathcal{D}} \phi_i d\mathbf{x} = 1$ for all $i = 1, \dots, n$. The parameter-to-observation map is then defined by $\mathcal{F} : \kappa \mapsto [B_1(\mathcal{S}(\kappa)), \dots, B_n(\mathcal{S}(\kappa))]^\top$. The coefficient κ is endowed with the distribution $\kappa \sim \mathcal{N}(0, \mathcal{C}(\mathbf{x}, \mathbf{x}'))$, where $\mathcal{C}(\mathbf{x}, \mathbf{x}') := \exp(-\|\mathbf{x} - \mathbf{x}'\|_2)$ is the Ornstein–Uhlenbeck (exponential) covariance kernel. Letting Σ be the discretization of \mathcal{C} over the finite element mesh, we define the likelihood to be $\mathcal{L}_\mathbf{y}(\mathbf{z}) \propto \exp\left(-\|\mathbf{y} - \mathcal{F}(\Sigma^{1/2}\mathbf{z})\|_{\Sigma_{\text{obs}}^{-1}}\right)$. We stress here that the model is computationally demanding: the evaluation of $\pi(\mathbf{z})$ and $\nabla \pi(\mathbf{z})$ require approximately 1 s.

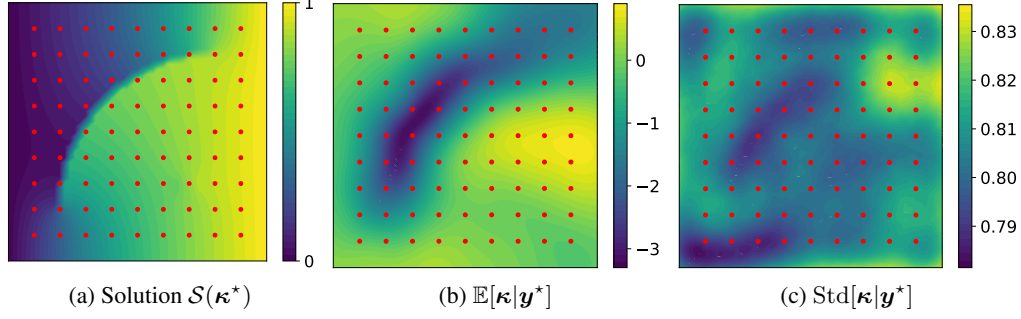


Figure 5: Additional figures for the elliptic problem with unknown diffusion coefficient. Figure (a) shows the solution u corresponding to the field in Figure 3a. Figures (b) and (c) show the mean and the standard deviation of the posterior distribution.

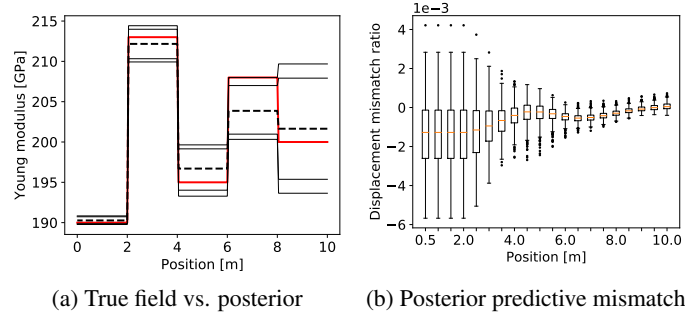


Figure 6: Additional results for the estimation of Young's modulus of a cantilever beam. Figure (a) shows the mean (dashed black) and the 5, 10, 90, 95-percentiles (thin black) of the marginals of $\pi(\mathbf{E}|\mathbf{y}^*)$ compared with the true values (red). Figure (b) shows the distribution of $(\mathbf{y}^* - \mathbf{y})/|\mathbf{y}^*|$, where \mathbf{y} is distributed according to the posterior predictive $\pi(\mathbf{y}|\mathbf{y}^*) = \pi(\mathbf{y}|\mathbf{E})\pi(\mathbf{E}|\mathbf{y}^*)$.

Figure 5 shows the observation generating solution $u^* = \mathcal{S}(\kappa)$, the posterior mean $\mathbb{E}[\kappa|\mathbf{y}^*]$ and the posterior standard deviation $\text{Std}[\kappa|\mathbf{y}^*]$.

D.2 Estimation of the Young's modulus of a cantilever beam

Parameters of the coupled PDE system (9) have the following meanings and values: $\nu = 0.28$ is the Poisson ratio, $\kappa = 5/6$ is the Timoshenko shear coefficient for rectangular sections, $A = wh$ is the cross-sectional area of the beam, and $I = wh^3/12$ is its second moment of inertia. In this example we fix the Poisson ratio, but one could think of it varying from material to material, and thus estimate it jointly with the Young's modulus.

Let \mathcal{S} be the map $\mathbf{E} \mapsto w$ delivering the solution to (9). Observations are gathered through the operator $B_i(w) := \int_0^l w \phi_i \, d\mathbf{x}$, where ϕ_i are defined the same way as in Appendix D.1 for locations $\{s_i := i \cdot 0.5\}_{i=1}^{20}$. Defining the parameter-to-observable map $\mathcal{F} : \mathbf{E} \mapsto [B_1(\mathcal{S}(\mathbf{E})), \dots, B_{20}(\mathcal{S}(\mathbf{E}))]^\top$, observations \mathbf{y} are assumed to satisfy the model $\mathbf{y} = \mathcal{F}(\mathbf{E}) + \epsilon$, where $\epsilon \sim \mathcal{N}(0, 10^{-6} \cdot I_{20})$ corresponds to 1 mm of measurement noise.

Figure 6 shows additional results for the problem.